ACCEPTED MANUSCRIPT

Electrode biasing maintains the edge shear layer at high density in the J-TEXT tokamak

Electrode biasing maintains the edge shear layer at high density in the J-TEXT tokamak

R. Ke[1], P. H. Diamond[2,3*], T. Long[1], M. Xu[1*], Z. P. Chen[4], L. Gao[4], Q. H. Yang[4], Y. H. Wang[4], X. Y. Zhang[4], L. Nie[1], T. Wu[1], J. M. Gao[1], D. Li[4], N. C. Wang[4], Z. J. Yang[4], Z. Y. Chen[4], Y. Pan[4], and X. R. Duan[1]

[1]*Center for Fusion Science, Southwestern Institute of Physics, Chengdu, Sichuan 610225, China*

[2]*Center for Astrophysics and Space Sciences, University of California San Diego, La Jolla, California 92093, USA*

[3]*Department of Physics, University of California, San Diego, California 92093, USA*

[4]*International Joint Research Laboratory of Magnetic Confinement Fusion and Plasma Physics, State Key Laboratory of Advanced Electromagnetic Engineering and Technology, School of Electrical and Electronic Engineering, Huazhong University of Science and Technology, Wuhan, 430074, China*

Email: kerui@swip.ac.cn

Abstract: Collapse of the edge flow shear as the line-averaged density approaches the Greenwald density limit has been observed as a precursor to the enhanced edge particle flux characteristic of proximity to the density limit regime. Here, we report the use of a biased electrode to sustain the edge shear layer in high density discharges, in which the shear layer would otherwise collapse. A stable increase in line-averaged density is observed along with a strong increase in edge density. These experiments were carried out on the J-TEXT tokamak. The Reynolds stress at the edge is enhanced, and the zonal flow sustained, while density perturbation levels, the flux of turbulence internal energy (i.e., turbulence spreading), and particle and heat flux all decrease significantly. Electron adiabaticity increases, and bias voltage modulation experiments show that an increase in the edge shear leads the increase in adiabaticity. These results suggest that external edge E×B flow shear drive may be of interest for sustaining edge plasma states at high density, and support the hypothesis that collapse of the edge shear layer triggers the onset of the strong transport and turbulence characteristic of the density limit regime.

Keywords: density limit, edge shear layer, turbulence, electrode bias

1. Introduction

High plasma density is desirable for fusion, and thus is part of the operating scenario for ITER and devices beyond. Intrinsic limits on density are thus of great interest. At present, the Greenwald (line-averaged) density scaling $n_G[10^{20}\text{m}^{-3}] = I_p[\text{MA}]/\pi a^2[\text{m}^2]$ is the empirical figure-of-merit for the density limit[1]. Note while the Greenwald scaling nominally applies to a line-averaged value, edge density is of great importance to fusion plasma performance[2], and so limits on edge density are of comparable interest.

The density limit has been investigated for decades, both by modeling and experiments (see Ref [1] and references therein), and has been found to be closely related to edge cooling. As density approaches the density limit, the plasma becomes unstable due to several different mechanisms. These mechanisms include enhanced (edge) turbulent transport [3][4], which leads to strong edge cooling, and thus triggers catastrophic MHD instabilities. Other mechanisms include MARFEs[5], as well as the growth of MHD[6]. The former is a radiative collapse resulting from the local imbalance between input power and radiation. The latter is a result of current profile shrinkage due to cooling by the radiating plasma. Edge cooling is due to a combination of enhanced particle convection losses and radiation[6]. Two or more mechanisms can work together and the details of their interplay are still open issues. Density limit phenomenology is complex, and reflects the interaction of enhanced edge turbulence and transport[3][4], edge cooling[6], radiation[7][8][9], MHD activity and disruption[6]. While the sequence of casual relations between all of these has yet to be established, enhanced edge turbulent transport is a good candidate for initiating edge cooling[12][18]. As $n \rightarrow n_G$, increased turbulent particle transport and stronger edge turbulence have been observed in various experiments[1][16][18][24]. These sometimes occur independent of the subsequent macroscopic evolution[10][11]. In these experiments, the edge shear layer collapses and strong turbulence spreading can be observed as $n \rightarrow n_G$. In terms of the shear flows-turbulence paradigm, this "density limit regime" emerges as one of the three basic states of the edge plasma, the other being the L-mode and the H-mode. In the L-mode, the edge turbulence has modest intensity and is regulated by zonal flows, and turbulence spreading is weak. In the H-mode, the edge turbulence and turbulence spreading both are very weak, and the edge turbulence is strongly regulated by mean shear flows.[12] The previous two-fluid simulation[13] and modeling work based on the AUG database [14] are consistent with this "three basic states of edge plasma". It has been suggested that the plasma enters the density limit regime when edge electron adiabaticity, $\alpha \equiv k_{||} v_{Th,e}^2 / |\omega| \nu_{ei}$, drops

below unity[12][15] (i.e., $\alpha < 1$), thus allowing the development of strong, fluid-like turbulence as opposed to, say, the expected drift wave turbulence with near-adiabatic electrons (i.e., $\alpha > 1$). Here, $k_{\parallel}$ denotes the parallel wavenumber, $v_{Th,e}$ is the electron thermal speed, v_{ei} is the electron–ion collision rate, and ω is the dominant frequency of turbulence. To this end, recent experiments[16] have linked the approach to n_G to a sharp drop in adiabaticity and the appearance of strong turbulence phenomena, such as spreading.

The question here, then, is how does this density limit regime develop—i.e., what triggers the onset of strong turbulence? A series of experiments together suggest that the collapse of the edge shear layer at high density[17][18][19] is of central importance. Recall that a shear layer is present at the edge of all L-mode tokamak and stellarator experiments[20][21][22]. As $n \rightarrow n_G$, LRC (long range correlation—indicative of zonal shear flow effects) and Reynolds power (i.e. the power exerted by the turbulence to drive the flow) are observed to drop, while concurrently, the particle flux and turbulence spreading (i.e. flux of fluctuation intensity) are observed to increase. The increase in spreading is likely indicative of increased density blob production[20], observed in earlier studies of density limit phenomenology[23]. Note that shear layer collapse is consistent with the reduced Reynolds stress-induced-production expected in regimes of low adiabaticity[12] or high collisionality[25]. More generally, the transition from L-mode to the density limit regime which occurs as the shear layer collapses is suggestive of a "back-transition" to a state of inferior particle confinement[26][27][28]. In this vein, the local E×B shearing rate emerges as a natural order parameter for the state of the edge[12], with strong mean shear indicating H-mode[12][30], normal zonal shear present in L-mode[30] and weak or no shear present in the density limit regime. This picture should be contrasted with others which invoke different linear instabilities to explain different plasma regimes[13][14].

The shear flow-as-order-parameter picture in turn begs the question of whether or not the L-mode edge shear layer can be maintained at high density by external means, and whether this sustained shear layer can control particle transport and allow access to yet higher density regimes? A straightforward, relatively simple means of shear layer sustainment is to use a bias probe inserted in the edge to drive sheared flow[31]. By inserting an electrode with high electric bias beyond the LCFS, a strong radial current is produced. This, in turn, drives poloidal rotation and so generates a sheared radial electric field, which then regulates edge turbulence and transport[17]. Suppression of edge turbulence and transport by biased electrode-driven shear flow has been observed previously on J-TEXT and other devices[32][33]. This improved confinement regime

is sometimes referred to as the "biased H-mode" state. However, most previous bias experiments have been performed at densities well below n_G. Thus, external control of the L-mode edge at high density represents a new application of electrode-bias-induced flow generation.

In this paper, we report on the use of a bias electrode to sustain the edge shear flow of J-TEXT as $n \rightarrow n_G$. Absent the bias, the edge shear layer is observed to collapse. However, with a positive bias of +240V, the edge Reynolds stress is enhanced and the zonal flows thus sustained. The level of edge density fluctuations $\langle (\tilde{n}/n)^2 \rangle$ is significantly lower than in the no-bias state, and the particle flux, electron heat flux and turbulence internal energy flux are also comparatively reduced. A stable state which manifests a modest increase in line-averaged density and a doubling of the edge density is maintained. With +240V bias, the electron adiabaticity is larger in comparison to the no-bias case. The study of the causality relation between edge flow shear and adiabaticity indicates that the evolution of edge flow shear leads the evolution of adiabaticity. In particular, the sense of the hysteresis loop is counter-clockwise. An asymmetry between positive (+240V) and negative (-240V) bias voltage was observed. More details are given in the Appendix A. These results are consistent with the hypothesis that edge shear layer collapse underpins the increase in edge particle transport, turbulence levels and turbulence spreading characteristic of the density limit regime. They also suggest that external edge E×B shear drive may be of interest for sustaining edge plasma states at high edge density. Moreover, for the shear-flow-as-order picture, these results indicate that an externally driven edge shear may prevent the edge plasma back transition from the L-mode to the density limit regime. This bolsters support for the key role of edge flow shear in density limit physics.

The remainder of this paper is organized as follows. Section 2 discusses the basic features of the experiments. Section 3 presents the results on how edge turbulence and transport vary with edge bias voltage. The impact of bias on the attainable density is addressed. Section 4 gives a Discussion and presents Conclusions.

2. Experiment setup

J-TEXT is a medium-sized tokamak device[34][35][36] with major radius $R = 1.05$ m and minor radius $a = 0.255$ m. In this paper, three positions of the top, bottom and outer limiters (Figure 1(a)) are used, and all three limiters is located at $r_{Limiter} = 25.5$ cm. The arrangement of the bias electrode and electrostatic probe is shown in Figure 1. The biasing electrode[37] is mounted in Port 8 on the midplane with a diameter of 40 mm and a thickness of 7 mm. The inner surface of the graphite electrode in these experiments stays at $r = 21.5$ cm. The bias electrode is powered by a set of adjustable
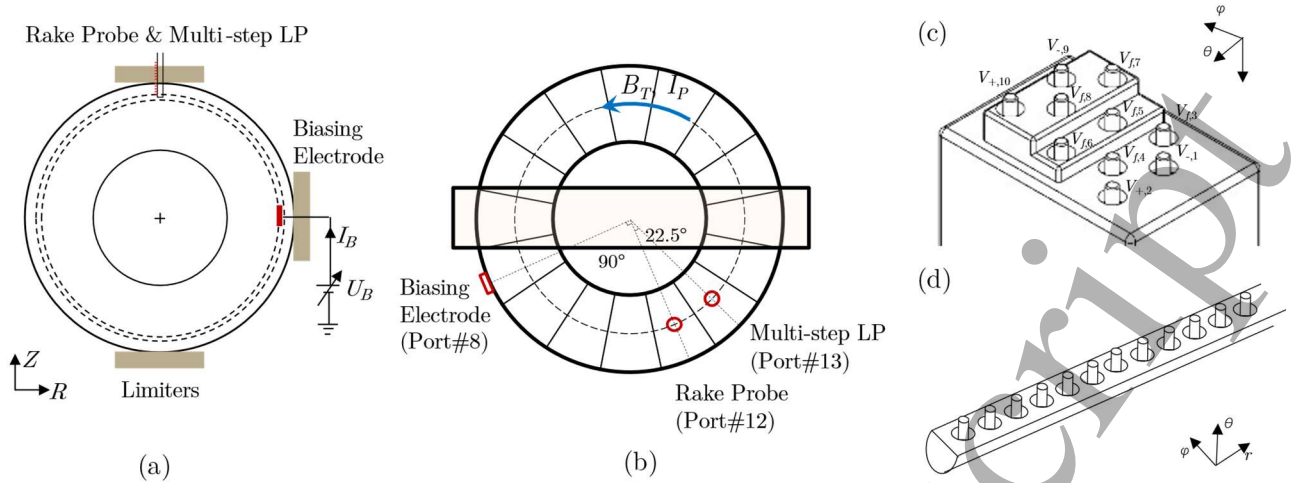
Figure 1 Arrangement of probes and biasing electrode. (a) Cross-section of J-TEXT tokamak, a = 25.5 cm. The bias electrode locates at r = 21.5 cm and the rake probe array was used for measuring floating potential at r - a = -1.75 to 2.65 cm. (b) Top view of J-TEXT tokamak, R = 1.05 m. Rake-probe and multi-step LP are toroidally separated by 22.5°. (c) The configuratioin of multi-step Langmuir probe array. Pin pairs ($V_{-,1}$,$V_{+,2}$) and ($V_{-,9}$,$V_{+,10}$) are double probe pairs, and other pins are floating. (d) Schematic view of the rake probe array. All of the 12 pins are floating.

DC constant-voltage power supplies, which could provide a maximum bias voltage of ±950 V and a maximum bias current of ±600 A. Two electrostatic probe arrays are mounted on two windows, Port#12 and Port#13, at the top of the device (Figure 1(a,b)), and are pushed by independent pneumatic propulsion systems to designated radial positions. These stay at fixed locations during the plasma discharge so as to monitor the changes of plasma parameters in the edge region during the plasma density rise. Among them, the Port#12 window is installed with a 12-pin rake probe array with a 4 mm radial pin spacing (Figure 1(d)). The rake probe array can monitor the evolution of the floating potential profile in the range of r - a = -1.75~2.65 cm during the discharges. The radial electric field may be inferred from $E_r = -\nabla_r \phi \approx -\nabla_r V_f - 3\nabla_r T_e/e$, where ϕ, V_f, T_e and e denote the plasma potential, floating potential, electron temperature and elementary charge, respectively. Since the electron temperature profile is flat— especially at the high densities (Figure 4 (a,c))—the second term, $-3\nabla_r T_e/e$, is negligible. Thus, the radial electric field can be estimated by the gradient of floating potential as $E_r \approx -\nabla_r V_f$. The Port#13 is installed with a 10-pin three-step probe array (Figure 1(c)), where the highest and lowest steps are four probe arrays[40][41], and the two pins on the middle step measure the floating potential. This configuration allows the probe to simultaneously obtain important parameters such as local electron temperature $T_e = (V_{+,10} - V_{f,8})/\ln2$, and ion saturation current $I_{sat} = (V_{-,9} - V_{+,10})/R_{shunt}$. Here, R_{shunt} refers to the sample resistor in the double probe circuit. $V_{+,10}$ is the potential of pin #10 which is connected to the anode of a 200V battery through the sample resistor.
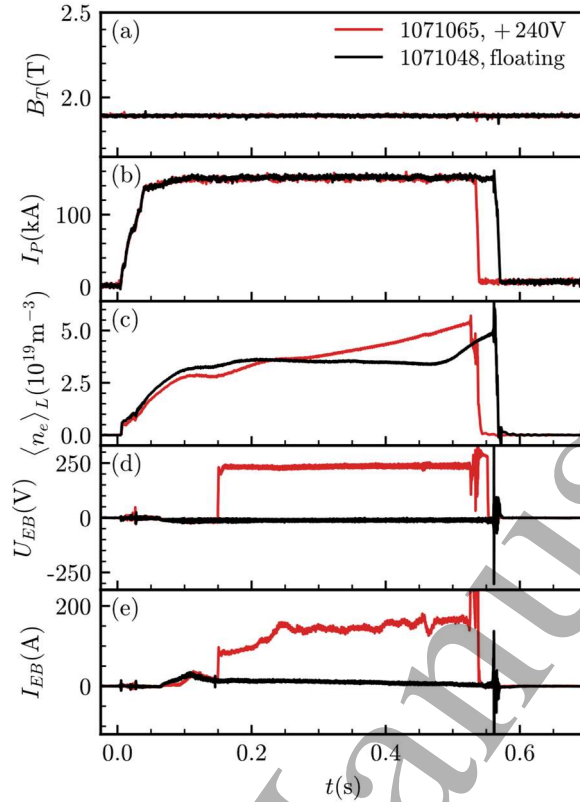
Figure 2 Time sequences of (a) toroidal field B_T, (b) plasma current I_p, (c) line-averaged density $\langle n_e \rangle$, (d) electrode biasing voltage U_{EB} and (e) driven biasing current I_{EB}. The red and black lines represent +240 V bias and floating electrode, respectively. The positive sign of I_{EB} denotes the electron current.

$V_{-,9}$ is the potential between the battery anode and the sample resistor. $V_{f,8}$ denotes the floating potential measured by pin #8. The electron density can be inferred as $n_e = I_{sat}/\left(0.49 e A_{eff}\sqrt{(T_e + T_i)/m_i}\right)$, where A_{eff} denotes the effective collection area of the pin #9, T_i is the ion temperature estimated as $T_i = T_e$, and m_i represents the ion mass. The radial and poloidal E×B velocity fluctuations, $\tilde{v}_{r,E\times B}$ and $\tilde{v}_{\theta,E\times B}$, are inferred and estimated as $\tilde{v}_{r,E\times B} = (\tilde{V}_{f,5} - \tilde{V}_{f,6})/\Delta_\theta B_T$, $\tilde{v}_{\theta,E\times B} = -(\tilde{V}_{f,8} - \tilde{V}_{f,4})/\Delta_r B_T$, where the $V_{f,4}$, $V_{f,5}$, $V_{f,6}$, denote the floating potentials of pin #4, #5, #6, respectively. Δ_θ denotes the poloidal distance between pin #5 and #6. And Δ_r denotes the radial distance between pin #4 and #8. In this paper (unless otherwise specified), the angular brackets, $\langle A \rangle$, mean averaging over 2 microseconds so as to obtain the equilibrium of quantity A. And the fluctuation of A, represented by $\tilde{A}$, is obtained by filtering A with a bandpass FIR digital filter. The passband is 1-200 kHz and the overlap with MHD instabilities at 8-12 kHz is filtered out. Reynolds stress, particle transport and thermal transport can be obtained using these measured parameters[16]. By means of a repeated discharge, shot-by-shot

-6-

scan, this three-stage probe obtains the evolution of the profiles with increasing plasma density within the edge region $r - a$ = -2 to 0 cm. All of the probe signals are sampled with a 2 Ms/s 14-bit multi-channel simultaneous digitizer. In addition, the J-TEXT device is equipped with a 17-channel FIR interferometer that measures the line-averaged density at different major radius locations and allows an inversion algorithm to be used to obtain the plasma density profile [42]. In particular, the line-averaged density, $\langle n_e \rangle_L$, used in this paper is obtained by the FIR channel at R_0 = 1.05 m.

Figure 2 shows the basic experiment setup. In the experiments of this paper, if not otherwise specified, the toroidal field B_T = 1.9 T, plasma current I_p = 155 kA, and q_a ~ 3.8 are used for the ohmic discharges. Continuous gas puffing is applied. In these experiments, the wall condition is high recycling at high densities, and no sign of detachment is observed. A bias voltage of +240 V is used to drive the bias currents (red lines in Figure 2(d,e)). When using positive bias, the biasing electrode collects primarily electron current, and the bias current gradually increases from +85 A to +180 A as the line-averaged density rises. Further increasing the bias voltage results in a larger bias current, indicating that the bias current has not yet reached the electron saturation current for +240 V bias voltage. However, at higher bias voltages and currents, the graphite electrode sputters severely, resulting in the loss of a stable discharge state. In the experiments, the discharge with bias electrode in the floating state, for which the bias current is approximately zero, is used as a reference (black lines in Figure 2).

3. Edge turbulence and transport

3.1 Edge shear layer sustained by electrode bias

Earlier experiments show that the edge shear flows collapse when the edge electron response transits from adiabatic ($\alpha \equiv k_{||} v_{Th,e}^2 / |\omega| \nu_{ie} \gg 1$) to hydrodynamic ($\alpha \ll 1$), as the line-averaged density of the plasma approaches the density limit[16][18]. In these J-TEXT experiments, collapse of the sheared radial electric field in the edge region was also observed as the line-averaged density increased in unbiased conditions. Figure 3 shows the evolution of the floating potential in the edge region and its negative radial gradient (an approximation of radial electric field E_r) profiles at different line-averaged densities, as monitored by the rake probe array (Figure 1). It can be seen that the sheared electric field within 0.5 to 1.5 cm of the LCFS collapses at high density (Figure 3(a,b)), similar to the phenomenon in Refs [16][18]. For the addition of +240 V bias voltage, the bias current drives a strong sheared electric field in the edge region, and the edge sheared electric field changes little as the line-averaged density increases. Figure 3(d) shows that the radial gradient of $-\nabla_r V_f$, i.e. E_r shearing rate, at r-a = -0.5 to -2 cm remains large or even increases as the line-averaged density increases.
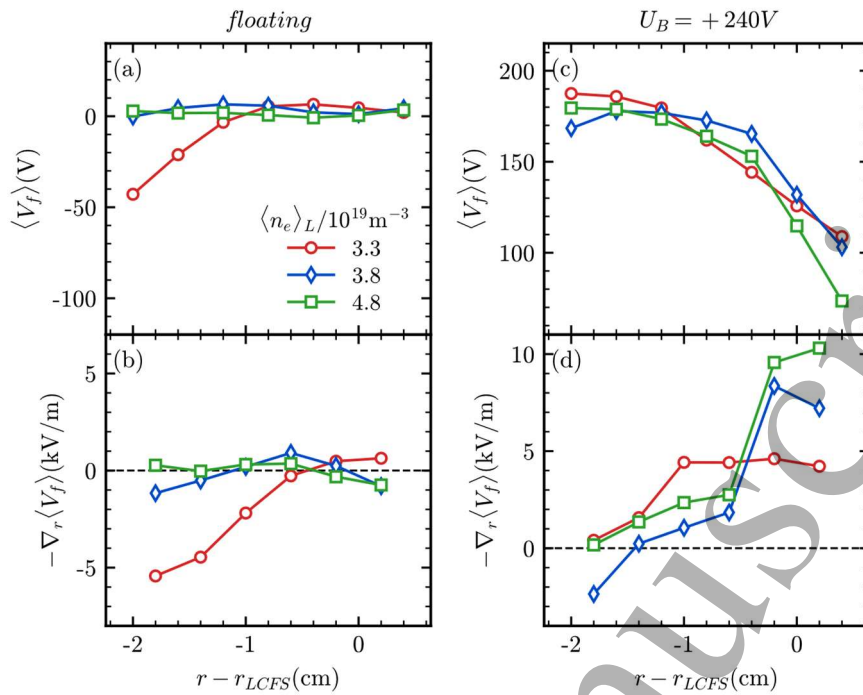
Figure 3 Profiles of (a) edge floating potential $\langle V_f \rangle$ for floating electrode, (b) negative gradient of $\langle V_f \rangle$ for floating electrode, (c) edge floating potential $\langle V_f \rangle$ for +240 bias voltage, and (d) negative gradient of $\langle V_f \rangle$ for +240 bias voltage. The floating potential profiles are obtained with the rake probe array. The red circles, blue diamonds and green rectangles represent three densities $\langle n_e \rangle_L$ = 3.3, 3.6, 4.8×10^{19} m^{-3}, respectively.

The electron temperature and density in the edge region are significantly influenced by the bias current. Figure 4 shows the plasma electron temperature T_e and density n_e profiles in the edge region obtained by the multi-step electrostatic probe via shot-by-shot scan, as the line-averaged density increases for the electrode floating and +240 V bias. For the condition of floating electrode, the electron density in the edge region changes little with the gradual rise of $\langle n_e \rangle_L$ (Figure 4(b)). The electron temperature gradually decreases from ~15 eV to ~10 eV (Figure 4(a)). Since the ionization energy of the hydrogen atom is about 13.6 eV, an edge temperature around 10 eV is a crucial sign of edge cooling by ionization and charge-exchange losses, and edge cooling is crucial to the density limit phenomenon [1][6]. When the electrode is applied with positive bias voltage, the electron temperature in the edge region is higher than when the electrode is floating at low density ($\langle n_e \rangle_L/n_G$ = 0.46) (Figure 4 (c)). When $\langle n_e \rangle_L$ gradually rises, the positive bias is able to maintain the plasma temperature around 20 eV in the edge region, especially at r-a = -0.5 to -1.5 cm, even though the electron density in the edge region has already risen significantly at this time. These observations indicate that with sufficient positive bias, a strong edge flow shear can reduce the edge cooling while approaching density limit.

-8-
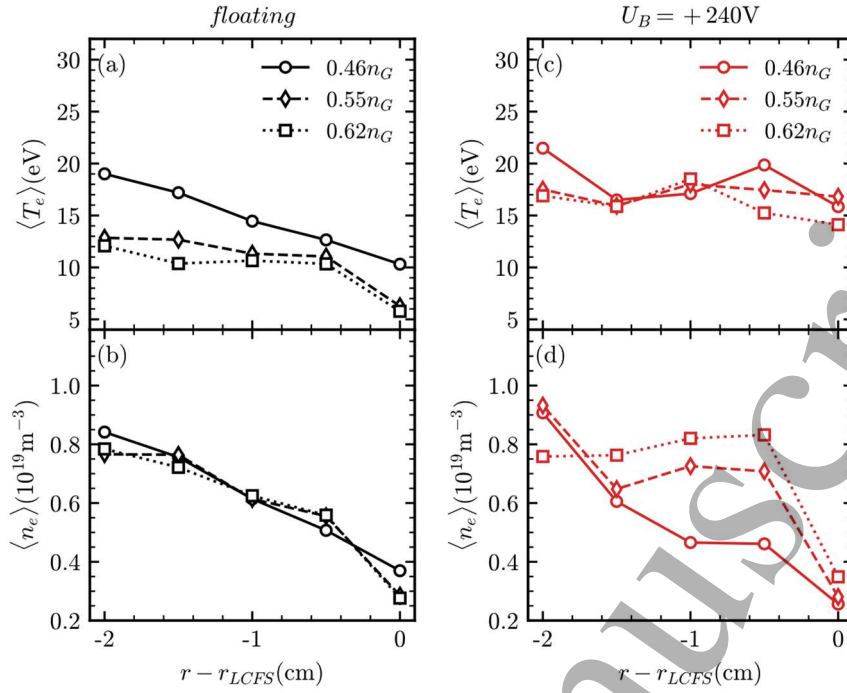
Figure 4 Profiles of (a) edge electron temperature $\langle T_e \rangle$ for floating electrode, (b) edge electron density $\langle n_e \rangle$ for floating electrode, (c) edge electron temperature $\langle T_e \rangle$ for +240 V bias, and (d) edge electron density $\langle n_e \rangle$ for +240V bias. The solid circle, dashed diamond and dotted square lines represent $\langle n_e \rangle_L =$ 0.46n_G, 0.55n_G, and 0.62n_G, respectively.

In the turbulence-shear flow regime, the zonal flows regulate the turbulence level. Turbulence is able to drive the edge zonal flows, generating a finite Reynolds stress in the edge region[44]. Figure 5 shows the evolution of the Reynolds stress $\langle \tilde{v}_{r,E\times B} \tilde{v}_{\theta,E\times B} \rangle$ generated by the edge turbulence and its radial gradient with the rise of the line-averaged density. When the electrode is floating, both the Reynolds stress intensity and its gradient in the edge region are low, and decay as the line-averaged density rises. This is consistent with the edge shear flow collapse observed in previous experiments[16][18]. However, when positive bias voltage is applied, the Reynolds stress and its gradient in the edge region are significantly enhanced, especially in the strong shear region where r - a = -0.5 ~ -1 cm. This can also be examined by the tilt of the turbulent eddies. Figure 6 shows the joint probability distribution functions (pdf) of the turbulent radial velocity perturbation $\tilde{v}_{r,E\times B}$ and the poloidal velocity perturbation $\tilde{v}_{\theta,E\times B}$ (normalized by standard deviation of $\tilde{v}_{r,E\times B}$ and $\tilde{v}_{\theta,E\times B}$, respectively) at r-r_{LCFS} = -0.5 cm for $\langle n_e \rangle_L = 0.62n_G$. When positive bias is added, this tilt and elongation feature is somewhat enhanced during the rise of the line-averaged density (Figure 6(b)). This results in the sustainment of the Reynolds stress and its gradient in the positive bias case.
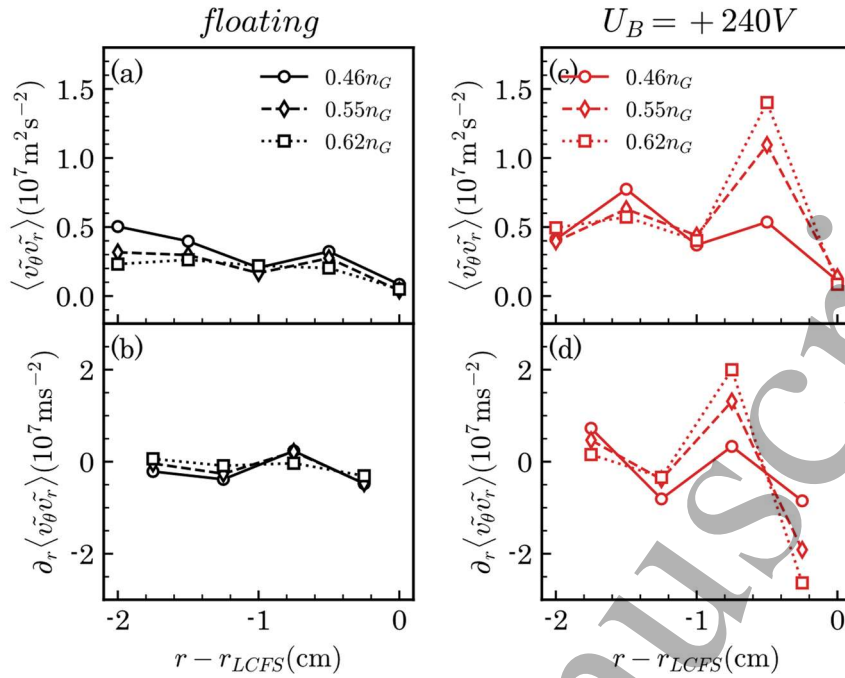
Figure 5 Profiles of (a) edge Reynolds stress for floating electrode, (b) radial gradient of Reynolds stress for floating electrode, (c) edge Reynolds stress for +240 V bias, and (d) radial gradient of Reynolds stress for +240V bias. The solid circle, dashed diamond and dotted square lines represent $\langle n_e \rangle_L = 0.46 n_G$, $0.55 n_G$, and $0.62 n_G$, respectively.

The enhancement of the Reynolds stress under the positive bias conditions is also reflected by the enhancement of zonal flows in the edge region. Geodesic acoustic modes (GAMs) have been observed in J-TEXT and have been well characterized[33]. The thermal GAM frequency can be expressed as $f_{GAM}^{th} = \sqrt{2(T_e + 7T_i/4)/m_i}/ 2\pi R_0$.[43] As measured by local Langmuir probes (Figure 4(c)), and assuming that the ion temperature is equal to the electron temperature, i.e., $T_i = T_e = 15\sim20$ eV, the thermal GAM frequency is estimated to be 14~16 kHz. This is consistent with the observed GAM fluctuation frequency, 13~19 kHz, as shown in Figure 7(b). For the floating electrode condition, GAMs are not observed in the edge region (Figure 7(a)). This is partly due to the small Reynolds stress driven by turbulence at high density mentioned earlier. It is also partly due to the low plasma temperature and high density in the edge region. These latter two lead to a high collision rate and thus an increase in the damping rate of GAMs. And when the bias voltage is applied, the intensity of GAMs in the edge region increases significantly (Figure 7(b)). Note that the enhanced Reynolds stress in the edge region contributes to an increase in the drive of GAMs[44]. The reduced collision rate due to higher plasma temperature in the edge region can reduce the damping of GAMs.
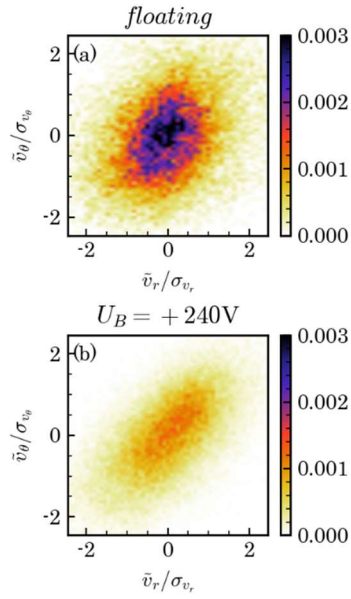
Figure 6 Joint pdf of normalized $\tilde{v}_{r,E\times B}$ and $\tilde{v}_{\theta,E\times B}$ for (a)floating electrode and (b)+240V bias at r-r_{LCFS} = -0.5 cm for $\langle n_e\rangle_L = 0.62n_G$. The subscripts in the labels are compressed for simplicity.
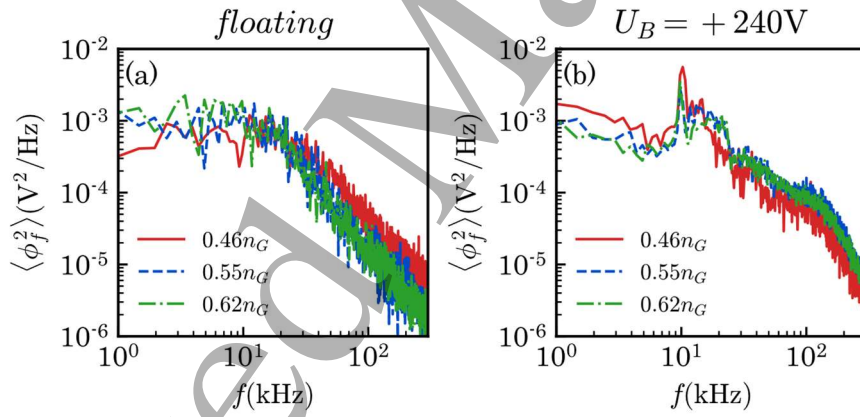
Figure 7 Spectrum of floating potential at r-a= -1 cm for (a)floating electrode and (b) +240V bias. The red solid lines, blue dashed lines and green dotted lines represent $\langle n_e\rangle_L = 0.46n_G$, $0.55n_G$, and $0.62n_G$, respectively. The frequency of GAMs is 13~19 kHz.

3.2 Turbulent transport regulated by electrode bias

The variation of the electron temperature and density profiles of the edge-region plasma is influenced by the particle and thermal transport in the edge-region. The anomalous transport due to turbulence is usually the dominant factor. Figure 8 (a) and (b) show the variation of the radial profiles of the relative perturbation of the ion saturation current $\delta I_{sat}/\langle I_{sat}\rangle$ and electron temperature $\delta T_e/\langle T_e\rangle$. These are shown
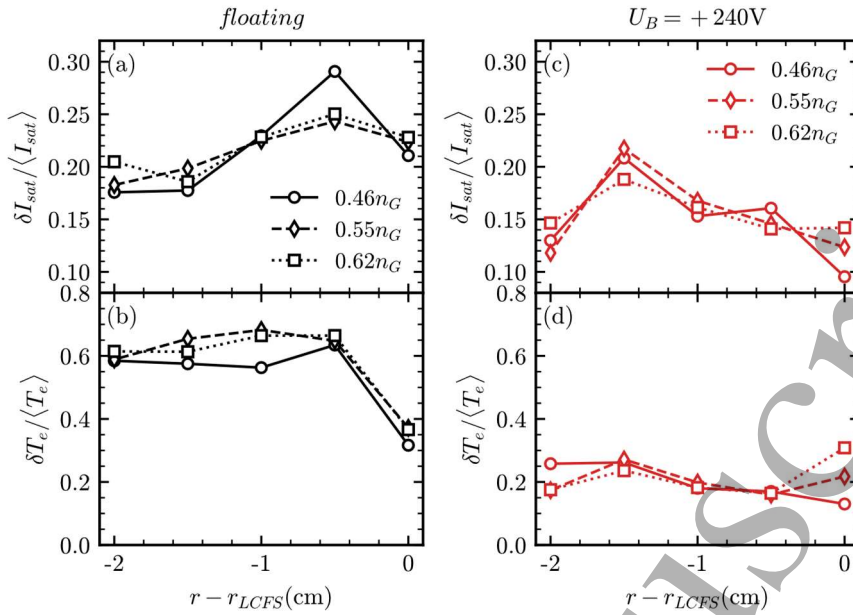
**Figure 8** Profiles of (a) the normalized perturbation intensity of ion saturation current, $\delta I_{sat}/\langle I_{sat}\rangle$, for floating electrode, (b) the normalized perturbation intensity of electron temperature, $\delta T_e/\langle T_e\rangle$, for floating electrode, (c) $\delta I_{sat}/\langle I_{sat}\rangle$ for +240 V bias and (d) $\delta T_e/\langle T_e\rangle$ for +240 V bias. The solid circle, dashed diamond and dotted square lines represent $\langle n_e\rangle_L = 0.46n_G$, $0.55n_G$, and $0.62n_G$, respectively.

for increasing line-averaged density with electrode floating, as obtained from the multi-step probe array (Figure 1(c)). $\delta I_{sat}/\langle I_{sat}\rangle$ and $\delta T_e/\langle T_e\rangle$ for the +240 bias case are shown in Figure 8(c) and (d), respectively. We compare the levels of ion saturation current perturbation and electron temperature perturbation for electrode floating with those for positive bias. This comparison shows that the sheared edge electric field induced by the biased electrode significantly reduces the perturbation intensity in the region of strong shear. The positive bias still exhibits some suppression effects even though the density gradually approaches the density limit.

Figure 9 shows the radial particle transport $\Gamma_n \equiv \langle\tilde{n}_e\tilde{v}_r\rangle$, turbulent thermal transport $q \equiv \frac{3}{2}\langle\tilde{n}_e\tilde{v}_r\rangle\langle T_e\rangle + \frac{3}{2}\langle\tilde{T}_e\tilde{v}_r\rangle\langle n_e\rangle$. As shown in Figure 9(a,c), with +240 V bias, the turbulent particle flux decreases in comparison to the floating case, indicating that there is clear improvement in the particle confinement. In Figure 9(b,d), the turbulent heat flux is observed to decrease with positive bias. Thus, thermal confinement also improves. Note that the electrode bias state differs fundamentally from the H-mode. In the H-mode, a strong *negative* electric field (E_r-*well*) is sustained. However, for the positive bias case, the E_r is *positive* and the strong E_r shear occurs near the LCFS (Figure 3(d)). The differences in E_r as well as turbulence profiles give rise to different T_e and n_e profile evolution. In this paper, the edge density profile changes from a steep

-12-
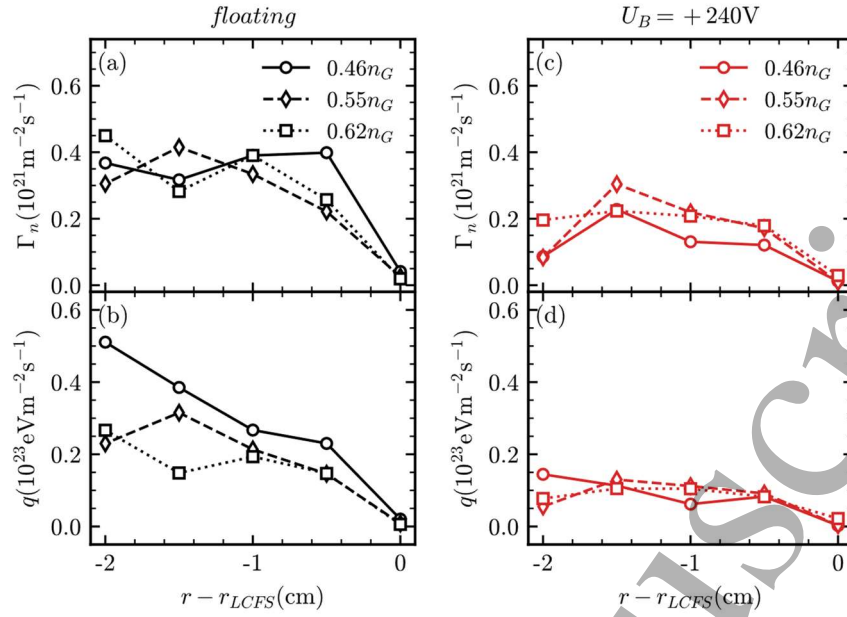
Figure 9 Profiles of (a) edge particle flux for floating electrode, (b) edge heat flux for floating electrode, (c) edge particle flux for +240 V bias, and (d) edge heat flux for +240V bias. The solid cricle, dash diamond and dot square lines represent $\langle n_e \rangle_L = 0.46 n_G$, $0.55 n_G$, and $0.62 n_G$, respectively.
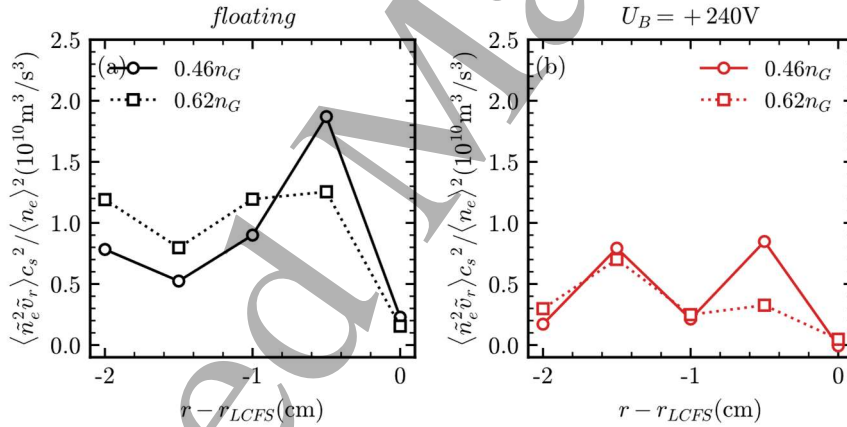
Figure 10 Evolution the flux of turbulence internal energy (turbulence spreading) for (a) electrode floating and (b) +240 V biasing. The solid circle lines and dotted square lines represent $\langle n_e \rangle_L = 0.46 n_G$ and $0.62 n_G$, respectively.

gradient to a flatter profile as $n \rightarrow n_G$ (Figure 4(d)). All of these are in sharp contrast to the conventional H-mode state. Figure 10 shows the evolution of internal energy flux ($\langle \tilde{n}^2 \tilde{v}_r \rangle c_s^2 / \langle n_e \rangle^2$, i.e. turbulence spreading) with increasing density for floating and positive bias voltage. The negative gradient of the internal energy spreading indicates the increase of the local turbulence internal energy through turbulence spreading. At +240V bias, the internal energy spreading and its gradient decrease significantly, as compared to the floating electrode case.

-13-
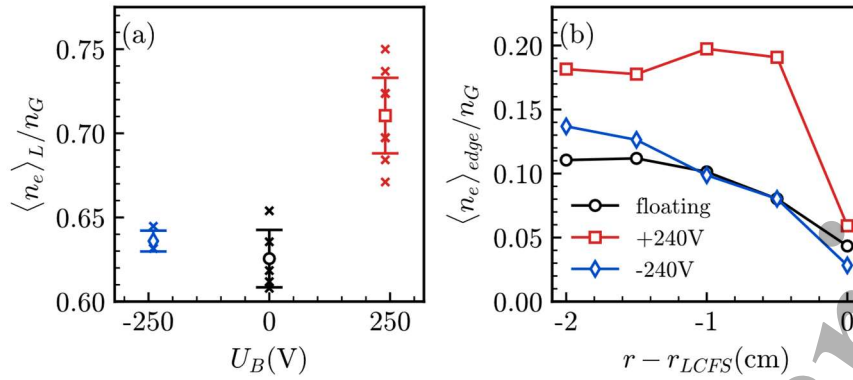
Figure 11 (a) The maximum density achieved before the plasma has a strong MHD or disruption with -240V (blue diamond) biasing, floating or 0V biasing (black circle), and +240V biasing (red rectangle). (b) The maximum edge density achieved before strong MHD or disruption with -240V (blue diamond) biasing, floating or 0V biasing (black circle), and +240V biasing (red rectangle).

3.3 Increase in $\langle n_e \rangle_L$ and $\langle n_e \rangle_{edge}$ with positive bias

The line-averaged density $\langle n_e \rangle_L$ at which the plasma manifests disruptive MHD activity varies for different bias conditions. Using the no-bias case as a reference, with +240 V bias, the disruption density obtained increased by ~8% (Figure 11(a)). On the other hand, the achievable edge density $\langle n_e \rangle_{edge}$, measured by the multi-step probe array (Figure 1(c)), increases significantly for +240 V bias in comparison to the floating electrode. The angular brackets in $\langle n_e \rangle_{edge}$ mean averaging over 2 microseconds right before the onset of disruptive MHD activity. Figure 11(b) shows the maximum edge density achieved before strong MHD or disruption occurs. For +240 V bias (red rectangles), the edge density is about twice that of floating electrode (black circles) at the edge shear layer of r - a = -0.5 ~ -1.5 cm. The high density accumulation in the edge may be a consequence of an inward particle pinch which is too small to balance the massive gas puffing and recycling when approaching the density limit [25]. This may partially explain why the line-averaged density cannot increase as much as the edge density for +240V bias. Furthermore, these results also are consistent with the view that the density limit (line-averaged) is strongly related to the edge density.

The effects of negative bias are not significant. This is due to the fact that the bias current driven by negative bias is too small compared to positive bias, which leads to a weaker radial electric field driven in the edge region. The negative bias is less effective in suppressing turbulence and its induced transport under high-density conditions, which ultimately leads to almost no significant change in the disruption density for negative bias. More details are given in Appendix.

### 3.4 Increase in α with positive bias
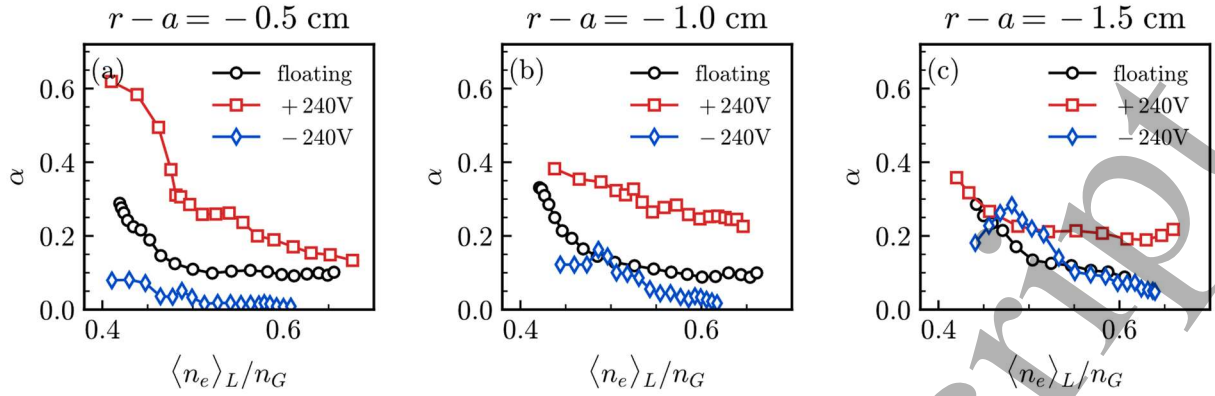
Figure 12 Electron adiabaticity α as a function of normalized line-averaged density $\langle n \rangle /n_G$ at (a) $r - a$ = -0.5 cm, (b) $r - a$ = -1.0 cm, and (c) $r - a$ = -1.5 cm. The black circles, red squares and blue diamonds denote electrode floating, +240V bias and -240V bias, respectively.

As mentioned above, earlier experiments and modeling have demonstrated the key role of electron adiabaticity in parameterizing the state of flow shear and turbulence. The electron adiabaticity $\alpha \equiv k_{||} v_{Th,e}^2 / |\omega| \nu_{ei}$ is estimated using local parameters. The parallel wavenumber is inferred as $k_{||} \sim 1/qR_0$, where q and R_0 represent the local safety factor and major radius, respectively. The dominant frequency of the turbulence is estimated to be ~25 kHz. This is obtained from the auto-power spectra of floating potentials ($V_{f,8}$ in Figure 1(c)) measured by the multi-step probe array, as shown in Figure 7(a,b). Figure 12(a)(b)(c) show the electron adiabaticity α as a function of normalized line-averaged density at r - a = -0.5, -1.0 and -1.5 cm. For the condition of floating electrode, α decreases to <0.1 as the line-averaged density increases. With +240V bias, α is much larger in comparison to the no-bias case. This is due to its strong dependence on temperature, though the edge density is higher[12][16][18][25]. For the -240V bias, α increases slightly at low density at r - a = -1.5 cm. However, similar to the no-bias case, α decreases rapidly to <0.1 as $n{\rightarrow}n_G$. These results suggest that sufficient edge flow shear driven by the positive bias can prevent or reduce the decrease of electron adiabaticity as $n{\rightarrow}n_G$.

To study the relations between the edge shear flows and electron adiabaticity, the response of α to the edge E×B velocity shearing rate, $\omega_s \equiv |\frac{\partial}{\partial r} v_{\theta, E \times B}|$, is investigated. Here $v_{\theta, E \times B}$ denotes the poloidal E×B flow velocity. ω_s is estimated as $|\frac{\partial^2}{\partial r^2} V_f / B_T|$, assuming that the temperature gradient is negligible. Thus, ω_s can be calculated from the floating potential profiles obtained by the rake probe array (Figure 1(d)). Figure 13 shows the trajectory of edge plasma in the ω_s-α phase space at $r - a = - 0.5$ cm while the +240V bias turned on and off in the bias modulation experiment (See more details

-15-

$$r - a = -0.5 \text{ cm}, \langle n_e \rangle_L / n_G = 0.61$$
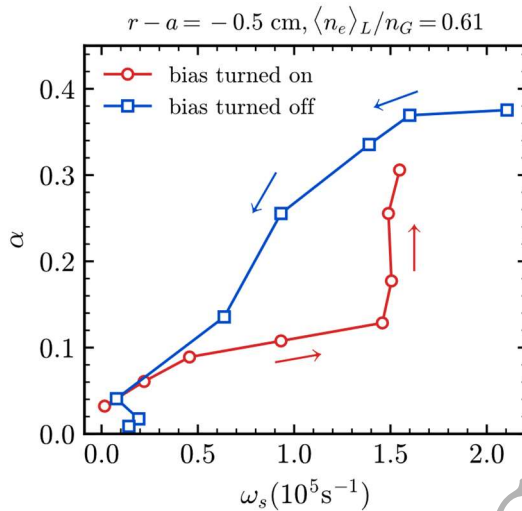
Figure 13 Trajectory of edge plasma in the ω_s-α phase space at $r - a = -0.5$ cm after the +240V bias turned on(red circles) and off (blue squares). The time interval between adjacent track points $\Delta t_w = 5$ μs.

in Appendix B). The trajectory rotates in the counter-clockwise direction, indicating that the evolution of ω_s leads that of α. This observation suggests the causality between edge shear flows and electron adiabaticity, i.e., that changes in adiabaticity follow changes in particle and heat transport induced by the edge shear.

4. Discussion and summary

By inserting an electrode with a high bias voltage into the main plasma of J-TEXT, a strong radial plasma current can be driven between the electrode and ground. This radial current sustains the edge shear flows as $n \to n_G$. These experiments compare the evolution of the plasma turbulence-shear flow system in the edge region for three states of floating electrode, -240 V bias, and +240 V bias. The experimental results show that

(1) Edge shear flows are sustained by +240V bias. Absent the bias, the edge shear layer is observed to collapse. However, with a positive bias of +240V, the edge Reynolds stress is enhanced and the zonal flows thus sustained.

(2) With positive bias, the level of edge density fluctuations $\langle (\tilde{n}/n)^2 \rangle$ is significantly lower than in the no-bias state, and the particle flux, electron heat flux and turbulence internal energy flux (i.e., spreading) also decrease.

(3) Edge cooling is reduced for +240V bias as $n \to n_G$. A stable state with a modest density increase is maintained. Somewhat higher line-averaged density limit of the plasma is observed for positive bias conditions (~8%). The achievable edge density is effectively doubled for +240 V bias, relative to the floating electrode case.

(4) With sufficient edge flow shear driven by +240V bias, the edge electron adiabaticity

-16-

decrease is reduced. The bias voltage modulation experiments show that the edge flow shear evolution leads that of adiabaticity.

(5) An asymmetry between positive (+240V) and negative (-240V) bias voltage is observed. Results for negative bias voltage are rather slight. See the Appendix for further details.

The positive bias drives strong poloidal shear flows, maintaining the edge shear layer at high density. The turbulence intensity, turbulent particle and heat transport and turbulence internal energy flux (turbulence spreading) all drop. Thus, edge cooling is reduced and a higher line-averaged density, along with a doubling of the edge density are observed. The observed evidence for the causality relation between edge flow shear and adiabaticity support the key role of edge flow shear in the transition from L-mode to density limit regime. These results support the hypothesis that collapse of the edge shear layer triggers the onset of the strong transport and turbulence characteristic of the density limit regime.

Nevertheless, there are other possibilities that may contribute to the reduction in the heat transport due to biasing. From the viewpoint of thermal equilibrium, lower heating power at higher temperature, and/or higher radiation loss at higher edge density may also result in reduction in heat transport. In this paper, the edge reduced turbulence and turbulent transport are presented, and clear reductions in turbulent particle transport and turbulent heat transport are observed. The effects of biasing on the thermal equilibrium are beyond the scope of this paper, and are well worth exploring in the future.

The aim of these experiments is to explore the use of externally driven E×B shear to sustain edge plasma states at high density. The results are promising. We should state that the density limit observed with bias here is not an intrinsic limit. In these experiments, the electron temperature near the electrode is estimated to be in the range of 50-200 eV. The consequent sputtering of the graphite electrode at this temperature is serious and is very likely to cause the surge in carbon impurity concentration in the plasma which we observed before disruption. The carbon sputtering problem of the graphite electrode also renders the electrode unstable at higher bias conditions, making it difficult to obtain higher bias currents. Since tungsten materials have a higher sputtering threshold[45], this suggests the use of a tungsten electrode will be able to relieve this problem and yield higher bias currents, thus leading to a more significant increase in the limiting density. Related work will be reported in subsequent studies.

Acknowledgement

ORCID IDs

R. Ke https://orcid.org/0000-0003-0117-0098

P.H. Diamond https://orcid.org/0000-0003-3273-2604

T. Long https://orcid.org/0000-0002-0136-8953

Z.P. Chen https://orcid.org/0000-0002-8330-0070

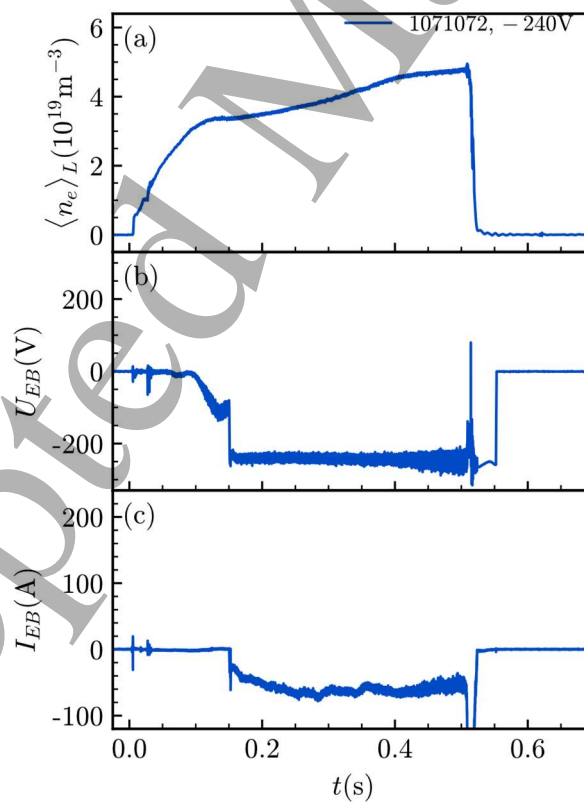N.C. Wang https://orcid.org/0000-0001-6797-2398
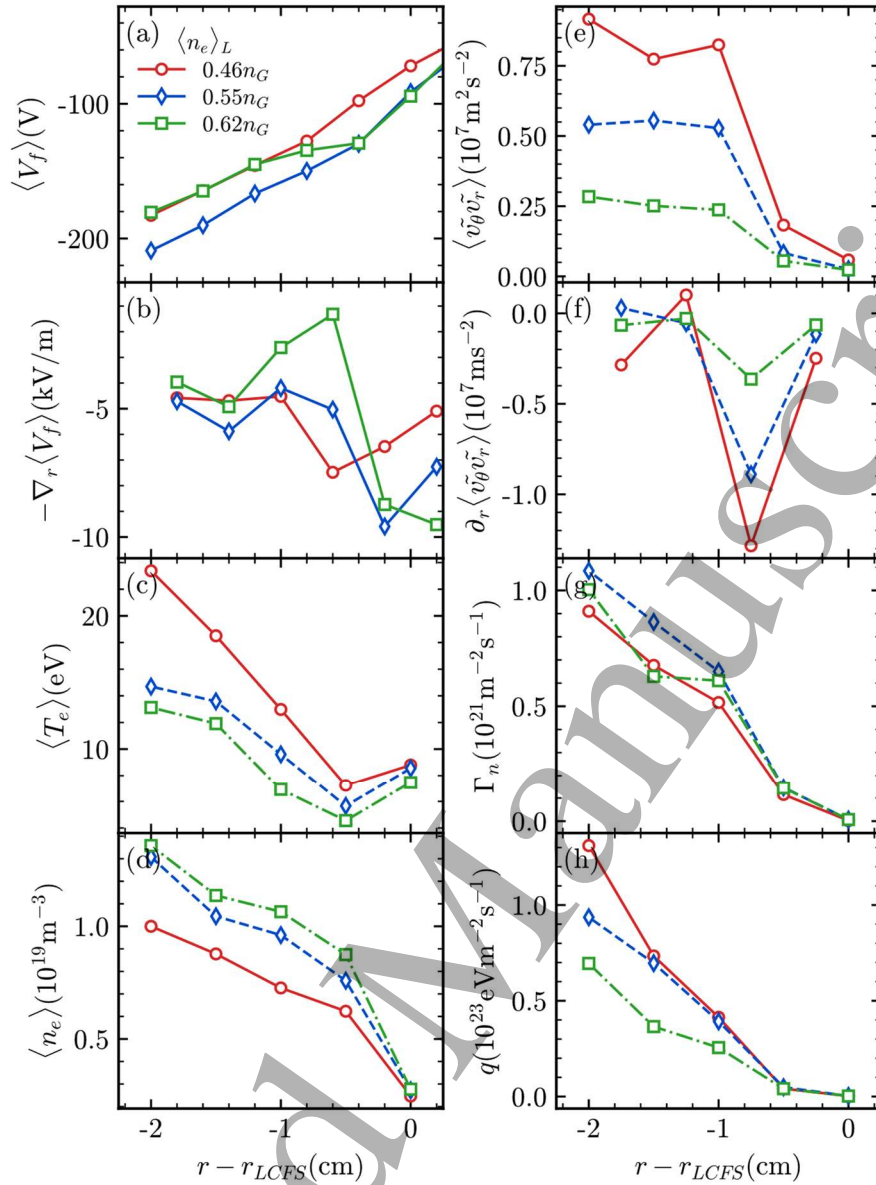
Z.Y. Chen https://orcid.org/0000-0002-8934-0364

Appendix A: Negative biasing electrode

Bias voltage of -240 V was also used to drive the bias currents (Figure A1). When

Figure A1 Time sequence of (a) line-averaged density $\langle n_e \rangle$, (b) electrode biasing voltage U_{EB} and (c) driven biasing current I_{EB} for +240V negative bias.

-18-

Figure A2 Evolution of edge profiles of (a) floating potential, and (b)radial gradient of floating potential, (c)electron temperature, (d) electron density, (e) Reynolds stress and (f)its gradient, (g)radial particle flux and (h) heat flux for -240 V biasing. The red solid, blue dashed and green dotted lines represent $\langle n_e \rangle_L = 0.46 n_G$, $0.55 n_G$, and $0.62 n_G$, respectively.

negative bias was used, the electrode collected primarily ion saturation current. As the plasma line-averaged density gradually increased from $3 \times 10^{19} \mathrm{m}^{-3}$ to $\sim 3.7 \times 10^{19} \mathrm{m}^{-3}$, the bias current driven by the negative bias voltage increased rapidly from -30 A to about -70 A. However, the bias current could not be increased more for further increase of the line-averaged density. The bias current is even slightly reduced when approaching the density limit ($\sim 5 \times 10^{19} \mathrm{m}^{-3}$). At this point, the bias current cannot be increased even if the bias voltage is further increased. This indicates that the bias voltage of -240 V is already sufficient to achieve the ion saturation current.

For negative bias conditions, the edge sheared electric field is stronger at lower densities, but as the density increases, the sheared electric field within the LCFS gradually disappears (Figure A2(a,b)). Thus, negative bias at high densities cannot maintain a strong sheared electric field in the edge region as it does for positive bias. This may be due to the fact that the negative bias drives a smaller ion saturation current, while the positive bias drives a larger electron current. The difference in sheared electric field driving capability will significantly affect the turbulent transport behavior in the edge region.

For the negative bias the electron temperature gradually decreases (Figure A2(e)). This shows the edge cooling phenomenon in the process of the approach to the density limit. When the negative bias electrode is applied, the electron temperature in the edge region is higher for -240V bias comparing to floating electrode at low density ($\langle n_e \rangle_L/n_G$ = 0.46). In contrast to the positive bias, negative bias performs similar to floating electrode case, in that it is difficult to prevent the electron temperature in the edge region from decreasing under high density conditions. Similar to the floating electrode, the negative bias cannot prevent the collapse of the edge shear flows.

The negative bias is also able to enhance the Reynolds stress and its gradient, but the enhancement decreases rapidly as the line-averaged density rises (Figure A2(e,f)), and the result is almost indistinguishable from that for the floating electrode near the density limit. The particle and heat flux are reduced only nearby the LCFS where the strong shear exist, while at r-a = -1.5 ~ -0.5 cm, the particle and heat flux are even stronger that those of floating electrode. The negative bias is less effective than positive bias at higher density conditions. As a result, the radial electric field formed in the edge region was not strong enough at -240 V and the density limit did not change significantly (Figure 11 blue diamonds).

Appendix B: Bias voltage modulation

In the bias voltage modulation experiments, the bias voltage is modulated between +240V and 0V. Figure B1 shows the time sequence of floating potential V_f, electron temperature T_e and ion saturation current I_{si} at r - a=-0.5 cm. The bias voltage was turned on at 0.25037s and turned off at 0.30050s. Data with 40 μs of turning on/off (shadowed region in Figure B1) is analyzed to investigate the relation between shear flow rate and adiabaticity. The shear rate is estimated via fitting of the floating potential profile measured by rake probe array, and adiabaticity is obtained by multi-step probe array (Figure 1).
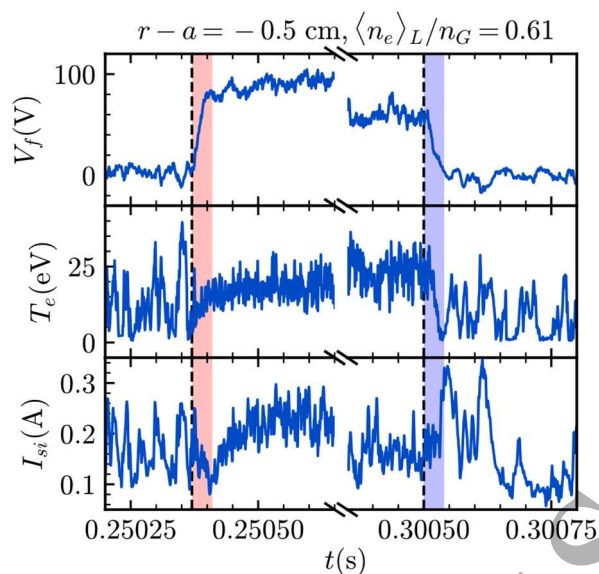
Figure B1 Time sequence of (a) floating potential V_f, (b) electron temperature T_e and (c) ion saturation current measured I_{si} by multi-step probe array at r - a= - 0.5 cm. The shadowed region denotes the data used in the Figure 13.

Reference

[1] Greenwald, M.. (2002). Density limits in toroidal plasmas. Plasma Physics and Controlled Fusion, 44(8), R27.

[2] Kamada, Y., Hosogane, N., Yoshino, R., Hirayama, T., & Tsunematsu, T. (1991). Study of the density limit with pellet fuelling in JT-60. Nuclear fusion, 31(10), 1827.

[3] Rapp J , Vries P C D , Schuller F C . Density limits in TEXTOR-94 auxiliary heated discharges[J]. Nuclear Fusion, 1999, 39(6):765.

[4] Brower D L, Yu C X, Bravenec R V, et al. Confinement degradation and enhanced microturbulence as long-time precursors to high-density-limit tokamak disruptions[J]. Physical review letters, 1991, 67(2): 200.

[5] F, Alladio, and, et al. The regime of enhanced particle recycling in high density tokamak discharges in the Frascati torus - ScienceDirect[J]. Physics Letters A, 1982, 90(8):405-409.

[6] Schuller F C. Disruptions in tokamaks[J]. Plasma Physics and Controlled Fusion, 1995, 37(11A): A135.

[7] Fielding S J, Hugill J, McCracken G M, et al. High-density discharges with gettered torus walls in DITE[J]. Nuclear Fusion, 1977, 17: 1382-1385.

[8] Zanca P, Sattin F, Escande D F, et al. A unified model of density limit in fusion plasmas[J]. Nuclear Fusion, 2017, 57(5): 056010.

[9] Zanca P, Sattin F, Escande D F, et al. A power-balance model of the density limit in fusion plasmas: application to the L-mode tokamak[J]. Nuclear Fusion, 2019, 59(12): 126011.

[10] LaBombard B, Boivin R L, Greenwald M, et al. Particle transport in the scrape-off layer and

its relationship to discharge density limit in Alcator C-Mod[J]. Physics of Plasmas, 2001, 8(5): 2107-2117.

[11] Greenwald M, Terry J L, Wolfe S M, et al. A new look at density limits in tokamaks[J]. Nuclear Fusion, 1988, 28(12): 2199.

[12] Hajjar R J, Diamond P H, Malkov M A. Dynamics of zonal shear collapse with hydrodynamic electrons[J]. Physics of Plasmas, 2018, 25(6): 062306.

[13] Giacomin M, Ricci P. Investigation of turbulent transport regimes in the tokamak edge by using two-fluid simulations[J]. Journal of Plasma Physics, 2020, 86(5).

[14] Eich T, Manz P. The separatrix operational space of ASDEX Upgrade due to interchange-drift-Alfvén turbulence[J]. Nuclear Fusion, 2021, 61(8): 086017.

[15] Rogers B N , Drake J F , Zeiler A . Phase Space of Tokamak Edge Turbulence, the L−H Transition, and the Formation of the Edge Pedestal[J]. Physical Review Letters, 1998.

[16] Long T, Diamond P H, Ke R, et al. Enhanced particle transport events approaching the density limit of the J-TEXT tokamak[J]. Nuclear Fusion, 2021.

[17] Xu Y, Carralero D, Hidalgo C, et al. Long-range correlations and edge transport bifurcation in fusion plasmas[J]. Nuclear fusion, 2011, 51(6): 063020.

[18] Hong R, Tynan G R, Diamond P H, et al. Edge shear flows and particle transport near the density limit of the HL-2A tokamak[J]. Nuclear Fusion, 2017, 58(1): 016041.

[19] Long T, Diamond P H, Xu M, et al. Studies of Reynolds stress and the turbulent generation of edge poloidal flows on the HL-2A tokamak[J]. Nuclear Fusion, 2019, 59(10): 106010.

[20] Ritz C P, Lin H, Rhodes T L, et al. Evidence for confinement improvement by velocity-shear suppression of edge turbulence[J]. Physical review letters, 1990, 65(20): 2543.

[21] Hidalgo C, Pedrosa M A, García L, et al. Experimental evidence of coupling between sheared-flow development and an increase in the level of turbulence in the TJ− II stellarator[J]. Physical Review E, 2004, 70(6): 067402.

[22] Grenfell G, van Milligen B P, Losada U, et al. The impact of edge radial electric fields on edge–scrape-off layer coupling in the TJ-II stellarator[J]. Nuclear Fusion, 2019, 60(1): 014001.6

[23] Manz P, Ribeiro T T, Scott B D, et al. Origin and turbulence spreading of plasma blobs[J]. Physics of Plasmas, 2015, 22(2): 022308.

[24] Greenwald M..20 years of research on the Alcator C-Mod tokamak[J]. Physics of Plasmas, 2014, 21(11):110501.

[25] Singh R, Diamond P H. Bounds on edge shear layer persistence while approaching the density limit[J]. Nuclear Fusion, 2021.

[26] Wagner F, Becker G, Behringer K, et al. Regime of improved confinement and high beta in neutral-beam-heated divertor discharges of the ASDEX tokamak[J]. Physical Review Letters, 1982, 49(19): 1408.

[27] Estrada T, Hidalgo C, Happel T. Signatures of turbulence spreading during the H–L back-

transition in TJ-II plasmas[J]. Nuclear Fusion, 2011, 51(3): 032001.

[28] Miki K, Diamond P H. Role of the geodesic acoustic mode shearing feedback loop in transport bifurcations and turbulence spreading[J]. Physics of Plasmas, 2010, 17(3): 032309.

[29] Burrell K H. Turbulence behavior in the presence of transport barriers[J]. Plasma physics and controlled fusion, 2006, 48(5A): A347.

[30] Lan T, Liu A D, Yu C X, et al. Spectral characteristics of geodesic acoustic mode in the HL-2A tokamak[J]. Plasma Physics and Controlled Fusion, 2008, 50(4): 045002.

[31] Taylor R J, Brown M L, Fried B D, et al. H-mode behavior induced by cross-field currents in a tokamak[J]. Physical review letters, 1989, 63(21): 2365.

[32] Sun Y, Chen Z P, Zhu T Z, et al. The influence of electrode biasing on plasma confinement in the J-TEXT tokamak[J]. Plasma Physics and Controlled Fusion, 2013, 56(1): 015001.

[33] Shen H G, Lan T, Chen Z P, et al. Observations of zonal flows in electrode biasing experiments on the Joint Texas Experimental tokamak[J]. Physics of Plasmas, 2016, 23(4): 042305.

[34] Zhuang G, Pan Y, Hu X W, et al. The reconstruction and research progress of the TEXT-U tokamak in China[J]. Nuclear Fusion, 2011, 51(9): 094020.

[35] Liang Y, Wang N C, Ding Y H, et al. Overview of the recent experimental research on the J-TEXT tokamak[J]. Nuclear Fusion, 2019, 59(11): 112016.

[36] Yonghua D, Zhongyong C, Zhipeng C, et al. Overview of the J-TEXT progress on RMP and disruption physics[J]. Plasma Science and Technology, 2018, 20(12): 125101.

[37] Zhu T Z, Chen Z P, Sun Y, et al. The construction of an electrode biasing system for driving plasma rotation in J-TEXT tokamak[J]. Review of Scientific Instruments, 2014, 85(5): 053504.

[38] Kuznetsov Y K, Nascimento I C, Silva C, et al. Long-distance correlations in TCABR biasing experiments[J]. Nuclear Fusion, 2012, 52(6): 063004.

[39] Van Oost G, Adamek J, Antoni V, et al. Turbulent transport reduction by E×B velocity shear during edge plasma biasing: recent experimental results[J]. Plasma physics and controlled fusion, 2003, 45(5): 621.

[40] Qayyum A, Ahmad N, Ahmad S, et al. Time-resolved measurement of plasma parameters by means of triple probe [J]. Review of Scientific Instruments, 2013, 84(12): 123502.

[41] Silva C, Gon Alves B, Hidalgo C, et al. Fluctuation measurements using a five-pin triple probe in the Joint European Torus boundary plasma [J]. Review of Scientific Instruments, 2004, 75(10): 4314-6.

[42] Shi P, Chen J, Gao L, et al. Far-forward collective scattering measurements by FIR polarimeter-interferometer on J-TEXT tokamak[J]. Review of Scientific Instruments, 2016, 87(11): 11E110.

[43] Conway G D, Smolyakov A I, Ido T. Geodesic Acoustic Modes in magnetic confinement devices[J]. Nuclear Fusion, 2021.

[44] Diamond P H, Itoh S I, Itoh K, et al. Zonal flows in plasma—a review[J]. Plasma Physics and Controlled Fusion, 2005, 47(5): R35.

[45] Eckstein W, Laszlo J. Sputtering of tungsten and molybdenum[J]. Journal of nuclear materials, 1991, 183(1-2): 19-24.